Communication in Physical Sciences, 2026, 13(2): 380-402

# Isotherm Evaluation and Performance Assessment of Bone Biochar at Varied Dosages for the Simultaneous Removal of PAHs and Heavy Metals

**Emmanuel O. Okorodudu*, Kenneth A. Ibe, Ivwurie Wisdom, Bamidele H. Akpeji, Andrew O. Onofuevure**

**Received: 09 January 2026/Accepted: 14 March 2026 /Published: 20 March 2026**
https://dx.doi.org/10.4314/cps.v13i3.4

***Abstract:*** *The co-contamination of soils with polycyclic aromatic hydrocarbons (PAHs) and heavy metals arising from petroleum exploration and spill incidents poses significant remediation challenges due to differences in their physicochemical behavior and environmental persistence. This study investigated the effectiveness of bone biochar (BB), produced through pyrolysis of cattle bone at 400 °C for 2 h, for the simultaneous removal of sixteen priority PAHs and selected heavy metals (Cd, Cr, Ni, and Pb) from crude oil–contaminated soil. Physicochemical characterization using scanning electron microscopy (SEM), Fourier transform infrared spectroscopy (FTIR), and X-ray diffraction (XRD) confirmed a porous carbonaceous structure enriched with crystalline hydroxyapatite phases, providing multiple adsorption sites. Batch remediation experiments were conducted using biochar dosages ranging from 2 to 10 g per 50 g of contaminated soil over a 21-day incubation period. Removal efficiencies increased significantly with dosage, achieving maximum reductions of 89.75% for total PAHs and 89.51% for Ni at 10 g amendment, alongside substantial removal of Cd, Cr, and Pb. Adsorption equilibrium data were evaluated using Langmuir, Freundlich, and Temkin isotherm models. The Langmuir model provided the best fit for PAHs ($R^2$ = 0.988), Cd ($R^2$ = 0.978), and Pb ($R^2$ = 0.989), indicating predominantly monolayer adsorption behavior, whereas the Freundlich model better described Cr ($R^2$ = 0.788) and Ni ($R^2$ = 0.920), suggesting heterogeneous surface adsorption. The results demonstrate that bone biochar is an efficient and sustainable adsorbent for multi-contaminant soil remediation, with performance strongly governed by amendment dosage and contaminant-specific adsorption mechanisms.*

***Keywords:*** *Bone biochar, Polycyclic aromatic hydrocarbons (PAHs), Heavy metals, Adsorption isotherm, Soil remediation*

**Emmanuel O. Okorodudu***
Department of Industrial Chemistry, Dennis Osadebay University, Asaba, Delta State, Nigeria
**Email:** emmanuel.okorodudu@dou.edu.ng
**http://orcid.org/0000-0002-4447-7383**

**Kenneth A. Ibe**
Department of Chemistry, Federal University of Petroleum Resources, Effurun, Delta State, Nigeria
**Email:** Ibe.Kenneth@fupre.edu.ng
**https://orcid.org/0000-0002-3121-7574**

**Ivwurie Wisdom**
Department of Chemistry, Federal University of Petroleum Resources, Effurun, Delta State, Nigeria;
**Email:** wivwurie@yahoo.co.uk
**http://orcid.org/0000-0001-7026-2805**

**Bamidele H. Akpeji**
Department of Science Laboratory Technology, Federal University of Petroleum Resources, Effurun, Delta State, Nigeria
**Email:** akpeji.honesty@fupre.edu.ng
**http://orcid.org/0000-0002-8404-6465**

**Andrew O. Onofuevure,**
Department of Industrial Chemistry, Dennis Osadebay University, Asaba, Delta State, Nigeria;

**Email:** andrew.onofuevure@dou.edu.ng;
http://orcid.org/0009-0006-1146-8145

## 1.0 Introduction

The significant contamination of soils with petroleum products, hydrocarbons and toxic heavy metals has now emerged as a major challenge to a good environment in oil-producing areas of the world (Akpanudo & Olabemiwo, 2024a,b). Petroleum exploration and refining activities have significantly increased environmental pollution worldwide, particularly in oil-producing regions where accidental spills and improper waste disposal persist In developing countries, remediation challenges are further intensified by limited access to cost-effective and sustainable treatment technologies. Polycyclic aromatic hydrocarbons (PAHs) are persistent, hydrophobic organic pollutants, which contain mutagenic and carcinogenic properties that been produced mostly through incomplete combustion and spill of crude oil. At the same time, a basic heavy metal such as Pb, Cd, Ni, Cr, and Zn are also common in the affected soils of crude oil because of the geogenic and anthropogenic petroleum activities (Awaka-Ama *et al*., 2024). These contaminants pose long-term ecological and human health risks through bioaccumulation, food-chain transfer, and groundwater contamination, thereby necessitating efficient remediation strategies. PAHs co-existence with heavy metals in contaminated matrices leads to a complicated procedure of remediation due to their opposite behavior as suggested by their physicochemical properties, movement patterns, and physical interactions within the soil systems (Meng *et al*., 2025; Wu *et al*., 2024).

Consequently, the development of environmentally benign and economically viable remediation technologies has become a major focus of contemporary environmental research (Eddy *et al*., 2024b). The traditional remediation methods such as soil washing, chemical oxidation, and thermal desorption, can be energy-intensive, expensive, and thus produce secondary pollution. On the contrary, adsorption-based remediation has been a topic that has attracted growing concern because of its operational simplicity, cost-effectiveness, and low environmental disturbance (Eddy *et al*., 2023a-c; Kelle *et al*., 2023; Ogoko *et al*., 2023). Biochar is one of the emerging adsorbents that has seen a lot of research due to its large adsorption surface, porosity, surface functional groups, as well as environmental friendliness (Bayar *et al*., 2024; Haris *et al*., 2024). Previous studies have demonstrated the effectiveness of plant-derived and agricultural waste biochars for pollutant adsorption; however, their performance often varies depending on feedstock composition and surface chemistry. Bone-derived biochar shows unique adsorption properties attributed to the mineral-rich compositions that mostly comprise of hydroxyapatite, alkaline surface chemistry, and high affinity to organic and inorganic contaminants. The heavy metal immobilization processes on the calcium phosphate matrix are ion exchange, surface complexation, and precipitation, whereby the porous carbonaceous structure enables hydrophobic and the p-p electron donor acceptor relationships apt with PAHs (Das, 2024; Meng *et al*., 2025). These two-fold mechanisms of adsorption put bone biochar as a potential material in multi-contaminants remediation (Meng *et al*., 2025; Yaashikaa *et al*., 2024). Compared with lignocellulosic biochars, bone-derived biochar offers enhanced mineral functionality due to its calcium phosphate content, which promotes simultaneous adsorption of organic and inorganic pollutants.

Although there have been rising reports about the effects of biochar on the elimination of contaminants, there are still some knowledge

gaps that have been identified as critical. Furthermore, limited studies have systematically evaluated how adsorbent dosage influences adsorption mechanisms and isotherm behavior under realistic soil conditions containing mixed contaminants. One, most researches center their attention on either organic or inorganic pollutants, and less has been made concerning competitive or synergistic adsorption in multi-contaminant systems. Second, although modeling of adsorption isotherm (especially of Langmuir, Freundlich, and Temkin) has been extensively used to model the equilibrium interactions, the research lacks knowledge on the dose of adsorbent and its effect on the parameters of adsorption isotherms and on the efficiency of the remediation of complex soil matrix (Akpanudo & Chibuzo, 2020; Akpanudo *et* al., 2024; Das, 2024; Rodrigues Viana *et al*., 2025; Wu *et al*., 2024). The dosage of adsorbent has a direct relationship with available sites in the surface, aggregation character, convection of contaminants as well as cost-effectiveness; hence, it is vital to optimize the dosage to ensure any useful scale of application.

In addition, the majority of the equilibrium experiments are carried out in simplified aqueous systems, which might not be a good representation of heterogeneity in the soil, natural organic matter interference, and contaminant competition interactions. Investigations conducted in real soil matrices are essential because soil heterogeneity, mineral interactions, and natural organic matter significantly influence adsorption efficiency compared with simplified laboratory systems.

Therefore, this study aims to evaluate the adsorption performance of bone biochar at varying dosages for the simultaneous removal of polycyclic aromatic hydrocarbons and selected heavy metals from crude oil-contaminated soil. The study specifically investigates adsorption behavior under different biochar dosage conditions to determine the relationship between adsorbent quantity and contaminant removal efficiency. Adsorption equilibrium data are further analyzed using Langmuir, Freundlich, and Temkin isotherm models to elucidate the mechanisms governing pollutant–biochar interactions. Unlike conventional studies focusing on single-contaminant systems, this research evaluates adsorption performance within a complex multi-contaminant soil matrix. Particular emphasis is placed on understanding how biochar dosage influences adsorption site availability, surface interactions, and contaminant competition dynamics. The outcomes are intended to support the optimization of biochar application strategies for sustainable soil remediation in petroleum-impacted environments.

## 2.0 Materials and Methods

### *2.1 Collection and Preparation of Sample*

All experiments were conducted under controlled laboratory conditions, and analytical procedures were performed following standard environmental analytical protocols to ensure reproducibility and data reliability.

/ Cattle bones, obtained from a municipal slaughterhouse, were first cleaned by manually stripping off any remaining tissues. The bones were collected fresh and transported in sealed polyethylene bags to prevent external contamination prior to processing.

They were then washed multiple times with hot water before being oven-dried at 105°C for 24 hours. The dried bones were subsequently pulverized using a mechanical grinder and sieved to achieve a particle size of 0.25 mm. Drying was performed to remove residual moisture and organic residues that could interfere with pyrolysis efficiency and biochar quality.

The resulting bone particles were stored in airtight containers until subjected to pyrolysis.

### *2.2 Bone Biochar Production*

Biochar was produced in a temperature-controlled muffle furnace. For each run, 50 g of prepared feedstock was weighed into covered ceramic crucibles to create oxygen-limited conditions. Oxygen limitation was maintained to promote carbonization while minimizing combustion and ash formation. The crucibles were placed in the furnace at room temperature, and pyrolysis was performed at 400 °C with a heating rate of 10 °C/min. The samples were held isothermally for 2 hours to ensure complete thermal conversion. After the residence time, the furnace was allowed to cool naturally. The biochar yield was recorded gravimetrically to evaluate thermal conversion efficiency. The resulting biochar was removed, gently ground with a mortar and pestle for homogeneity, and stored in airtight containers for characterization.

### *2.3 Physicochemical Characterization of Bone Biochar*

To elucidate the physicochemical properties and surface characteristics responsible for adsorption behavior, the prepared bone biochar was characterized using Scanning Electron Microscopy (SEM), Fourier Transform Infrared Spectroscopy (FTIR), and X-Ray Diffraction (XRD), respectively. These characterization techniques were selected to relate structural, chemical, and mineralogical properties of the biochar to its adsorption performance. Instrument calibration was performed before analysis to ensure imaging accuracy.

#### *2.3.1 Scanning Electron Microscopy (SEM)*

12 mg of each sample was mounted on aluminum stubs using carbon adhesive tape and sputter-coated with a thin gold layer for 2 minutes to enhance surface conductivity and minimize charging during analysis. SEM imaging was performed using a high-resolution field emission scanning electron microscope (e.g., JEOL JSM-7600F) operated at 15–20 kV. Micrographs were captured at magnifications ranging from ×500 to ×30,000 using secondary electron mode to examine surface morphology, porosity, and particle clustering. Multiple fields of view were analyzed per sample to ensure representative microstructural assessment. Features such as pore structure, surface cracks, and carbonaceous residues were compared across biochar types (yam peel, bone, and composite). Differences in pyrolysis temperature and feedstock were linked to variations in pore morphology and surface area. Image processing software (e.g., ImageJ) was used to estimate pore dimensions and qualitative porosity. These observations supported correlations between surface characteristics and adsorption performance, which may help in PAH and some heavy metal removal, providing insight into carbonization quality and microstructural stability. SEM observations provided qualitative evidence of surface heterogeneity and pore development relevant to adsorption processes.

#### *2.3.2 Fourier Transform Infrared Spectroscopy (FTIR)*

Before analysis, biochar samples were dried at 60 °C in an oven to remove moisture. Each sample was then ground into a fine powder using an agate mortar and pestle. For pellet preparation, approximately 2 mg of biochar was mixed homogenously with 200 mg of dried KBr (1:100 ratio) and compressed into a transparent pellet using a hydraulic press at 10 tons of pressure for 2 minutes. Alternatively, some powdered samples were analyzed directly using an Attenuated Total Reflectance (ATR) accessory. Spectra were acquired using a Bruker Alpha II FTIR spectrophotometer in the mid-infrared region (4000–400 $cm^{-1}$) at a resolution of 4 $cm^{-1}$ over 32 scans.Spectral interpretation was carried out using established functional group assignment references reported in biochar characterization literature.

A background spectrum was recorded before each measurement to eliminate interference. Functional groups such as –OH, C=O, C–O–C, C–H, and aromatic C=C were identified based on characteristic absorption bands. Spectral

data were processed using software (e.g., OriginPro) to determine peak positions and intensities. The presence of oxygen-containing groups, particularly carboxyl and hydroxyl functionalities, indicated active adsorption sites. These functional groups were correlated with the biochar's reactivity, which plays a key role in the sorption and degradation of PAHs and selected heavy metals.

### *2.3.3 X-Ray Diffraction (XRD)*

XRD analysis was conducted to determine the crystalline or amorphous nature of the biochar samples. Prior to analysis, visibly moist samples were dried in an oven at 105 °C for 12 hours to remove residual moisture. The dried samples were then lightly ground into a fine powder and placed into a low-background quartz sample holder. Diffraction patterns were recorded using a Rigaku Ultima IV diffractometer operating at 40 kV and 30 mA with Cu Kα radiation (λ = 1.5406 Å). Measurements were performed over a 2 range of 5–80° at a scanning speed of 2°/min with a step size of 0.02°. The sample stage was spun continuously to ensure uniform exposure to the incident beam. Raw diffraction data were analyzed using software (PANalytical X'Pert HighScore) to identify crystalline phases and assess the degree of graphitization. Peaks observed at approximately -26.5 and -43 2 were attributed to disordered graphitic forms corresponding to the 002 and 100 planes, characteristic of carbonized materials. Sharp peaks in bone-derived biochar indicated the presence of hydroxyapatite [$Ca_{10}(PO_4)6(OH)_2$], while broad humps in yam peel biochar reflected its amorphous structure. Phase identification was confirmed by comparison with standard reference patterns from the International Centre for Diffraction Data (ICDD) database.

These findings provided key insights into the structural integrity and mineral composition of each biochar sample. The degree of crystallinity was directly related to thermal stability and reusability, while mineral phases were identified as potential contributors to adsorption through ion exchange or co-precipitation mechanisms.

### *2.4 Dosage Experimental Design*

The experimental design was structured to evaluate the influence of adsorbent dosage on contaminant removal efficiency and adsorption equilibrium behavior.

A dosage experiment was carried out to determine the optimal application rate of bone biochar for remediating crude oil contaminated soil. 50 g of air-dried, sieved soil was contaminated with 5 mL of crude oil and amended with 2, 4, 6, 8, and 10 g of bone biochar. The mixtures were thoroughly homogenized and incubated under ambient laboratory conditions for 21 days. A contaminated soil sample without biochar amendment served as the control. Soil moisture content was maintained at approximately field capacity throughout incubation to simulate natural environmental conditions.

All treatments were conducted in duplicate, giving a total of twelve experimental units. After incubation, the soils were analyzed to determine the removal efficiency of polycyclic aromatic hydrocarbons (PAHs) and selected heavy metals (Cd, Cr, Ni, and Pb).

### *2.5 Determination of Polycyclic Aromatic Hydrocarbons (PAHs) and Selected Heavy Metals (Cd, Cr, Ni, and Pb)*

Analytical measurements were performed in accordance with standard environmental monitoring procedures to ensure accuracy and comparability with existing studies. . The concentrations of polycyclic aromatic hydrocarbons (PAHs) in the incubated and remediated soil samples were determined using gas chromatography mass spectrometry (GC-MS) after solvent extraction. Approximately 10g of air dried, homogenized soil was extracted with a dichloromethane/hexane 1:1 (v/v) mixture using ultrasonic-assisted

extraction. The extract was filtered, concentrated with a rotary evaporator, and purified through a silica gel column. The cleaned extract was then analyzed by GC–MS, where PAHs were separated in the gas chromatograph and identified based on retention times and characteristics mass to charge ratios (m/z). Quantification was performed by comparing peak areas with external PAH standards, enabling sensitive detection of trace PAHs in the soil samples.

While, the concentrations of selected heavy metals **(**Cd, Cr, Ni, and Pb**)** in the soil were determined following acid digestion of the soil matrix. Approximately 2 g of dried and sieved soil was digested using a mixture of concentrated analar grade perchloric acid ($HClO_4$) purchased from BDH Laboratory Supplies, Poole England); analar grade nitric acid ($HNO_3$) purchased from Sigma-Aldrich, Ontario, Canada; and anala grade concentrated sulphuric (VI) acid ($H_2SO_4$) in the ratio 1:2:2 respectively under controlled heating to ensure complete dissolution of the metals. The digest was filtered and diluted to 50mL with deionized water. The resulting solution was analyzed using Atomic Absorption Spectrophotometry (AAS), and metal concentrations were calculated from calibration curves prepared with standard solutions, taking the dilution factor into account.

### *2.6 Adsorption Isotherm Modeling*

Adsorption isotherm models were employed to describe the equilibrium interaction between contaminants and bone biochar, as well as to assess the adsorbent's capacity and underlying mechanism. Equilibrium experiments were performed by applying varying amounts of bone biochar to soil samples contaminated with polycyclic aromatic hydrocarbons (PAHs) and heavy metals. Following equilibration, residual contaminant concentrations were measured, and the adsorbed amount was calculated using the equation:

$$q_e = \frac{(C_0 - C_e)}{m} \times \frac{V}{1} \quad (1)$$

where $q_e$ is the equilibrium adsorption capacity, $C_0$ and $C_e$ are the initial and equilibrium concentrations, and m is the adsorbent mass.

The adsorption data were fitted to Langmuir, Freundlich, and Temkin Isotherm models.

#### *2.6.1 Langmuir Isotherm Model*

The Langmuir model were used to assume adsorption occurs as a monolayer on a homogeneous surface bearing a fixed number of identical sites. The linear form of this model is expressed as:

$$\frac{C_e}{1_e} = \frac{1}{Q_m k} + \frac{C_e}{Q_m} \quad (2)$$

where $C_e$ is the equilibrium concentration, $q_e$ is the amount adsorbed at equilibrium, $Q_m$ is the maximum adsorption capacity, and K is the Langmuir adsorption constant.

A plot of $C_e/q_e$ versus $C_e$ was used to determine the Langmuir parameters.

#### *2.6.2 Freundlich Isotherm Model*

The Freundlich isotherm model accounts for adsorption onto heterogeneous surfaces characterized by non-uniform energy distribution among adsorption sites. Its linearized form is given by the equation:

$$logq_e = logk_F + \frac{1}{n} logC_e \quad (3)$$

where $K_F$ = Freundlich adsorption constant indicating adsorption capacity, n= adsorption intensity, qe = adsorption capacity at equilibrium and Ce = equilibrium concentration

A plot of log $q_e$ versus log $C_e$ was used to to test for the finess of this model and to estimate the balues of $K_F$ and n from the intercept and slope respectively.

#### *2.6.3 Temkin Isotherm Model*

The Temkin isotherm model incorporates adsorbent–adsorbate interactions and proposes a linear decrease in the heat of adsorption with progressive surface coverage. Its linearized equation is given by equation 4

$$q_e = Blnk_T + BlnC_e \quad (4)$$

where B = RT/b, $K_T$ = Temkin equilibrium binding constant (L $g^{-1}$), b = Temkin constant

related to heat of adsorption (J $mol^{-1}$), R = universal gas constant (8.314 J $mol^{-1}$ $K^{-1}$) and T = absolute temperature (K)

A plot of $q_e$ versus ln $C_e$ was apply to confirm the fitness of the Temkin models to the adsorption data and to estimate the Temkin adsorption parameters.

***2.6.4 Model Evaluation***

Evaluation of the adsorption isotherm models involved comparing their $R^2$ values, standard errors, and the agreement between experimental and theoretical adsorption capacities. The model that exhibited the highest $R^2$ and best matched the experimental data was considered the most suitable for describing the adsorption of PAHs and heavy metals on bone biochar.

**3.0 Results and Discussion**

***3.1 Characterization of Biochar***

Biochar characterization was conducted to determine structural and chemical properties responsible for adsorption behavior and to establish correlations between material composition and contaminant removal efficiency.

***3.1.1 Scanning Electron Microscopy (SEM)***

The bone biochar micrograph (Image D) reveals smoother surfaces with fewer cavities, indicating denser mineral phases resulting from complete carbon decomposition.The observed morphology indicates successful thermal transformation of organic bone components into minera-rich biochar matrices during pyrolysis. This morphology reflects enhanced hydroxyapatite crystallization, contributing to greater rigidity and chemical resistance. Although smoother surfaces reduce specific surface area, the remaining mineral phases facilitate alternative sorption mechanisms for heavy metals including $Pb^{2+}$, $Cu^{2+}$, and $Cd^{2+}$ through surface complexation with phosphate groups, ion exchange with $Ca^{2+}$ in the apatite lattice, and chemical precipitation of insoluble metal phosphates (Yang *et al*., 2019; Chen *et al*., 2022). These mineral-mediated interactions also enable adsorption of polar PAH derivatives or co-contaminants. Similar morphological contrasts between organic and inorganic domains of bone-derived biochar have been reported to influence sorption kinetics and pollutant-binding heterogeneity (Mei *et al*., 2022). Such mineral-dominated surfaces shift adsorption mechanisms from purely physical adsorption toward chemically controlled immobilization processes.

These structural characteristics suggest that adsorption efficiency is governed more by chemical reactivity than by surface area alone.

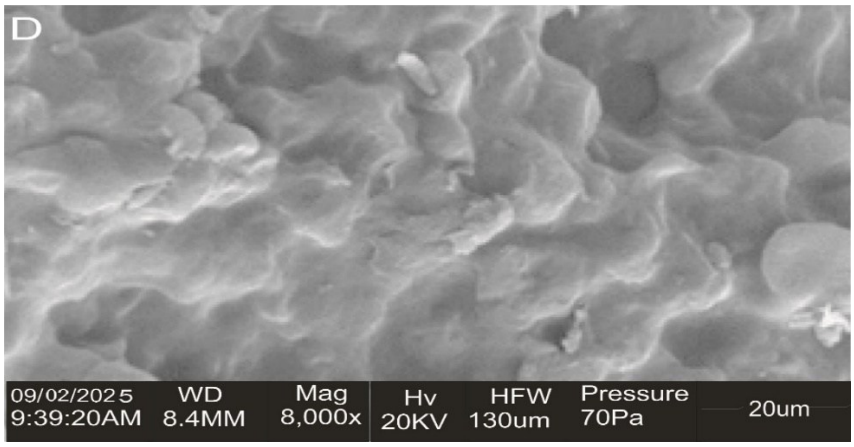


**Fig. 1: Scanning Electron Microscopy (SEM) micrograph of biochar obtained from bone.**

### *3.1.2 Fourier Transform Infrared Spectroscopy (FTIR)*

Bone biochar's FTIR spectrum shown in Fig. 1 is distinctly characterized by dominant mineral features with hydroxyapatite as the key component.The dominance of inorganic vibrational bands confirms extensive degradation of proteinaceous components during pyrolysis.

Sharp phosphate vibrations (P–O stretching: 1200–1000 $cm^{-1}$; O–P–O bending: 650–500 $cm^{-1}$) confirm a crystalline apatite structure formed after pyrolysis eliminated the original collagen matrix (Li *et al*., 2019; Vassilev *et al*., 2013). This phosphate-rich framework confers strong heavy metal adsorption through dissolution-precipitation (forming stable minerals like pyromorphite), ion exchange with lattice calcium, and surface complexation (Wang *et al*., 2026). However, phosphate groups contribute little to PAH removal, which may occur via adsorption onto residual carbonized material or physical pore trapping (Li *et al*., 2019). Weak organic signals (aliphatic C–H, aromatic C=C) indicate extensive decomposition of organic matter, leaving a thermally stable mineral structure with important practical implications. This observation highlights the complementary role of residual carbon domains in facilitating organic pollutant adsorption.

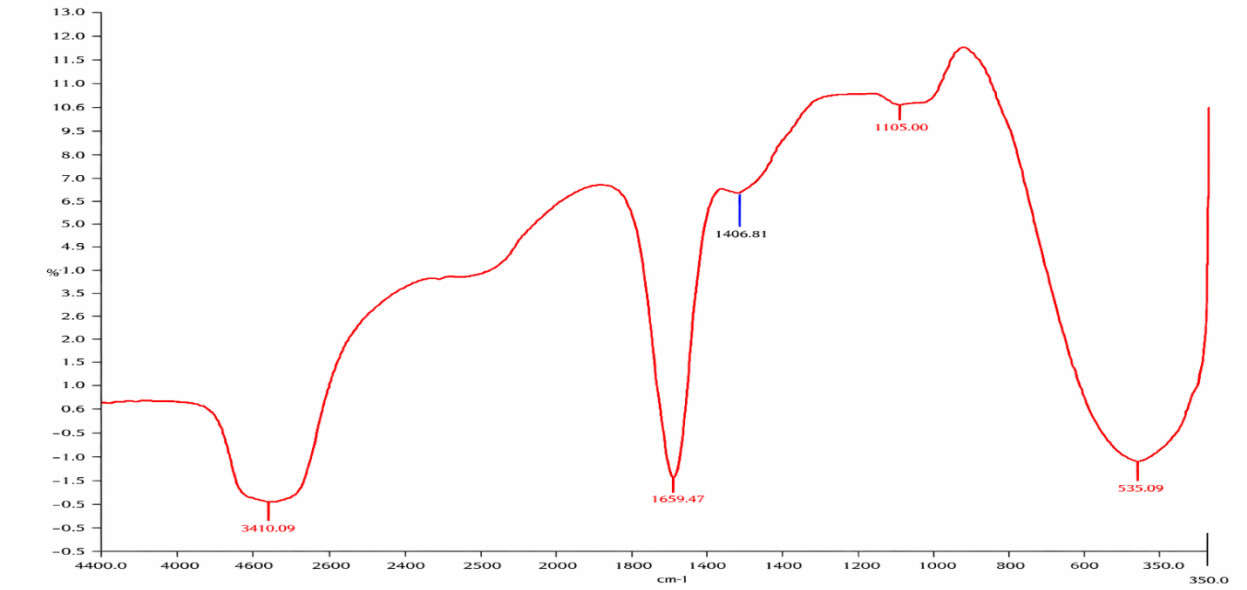


**Fig. 2: FTIR spectrum of biochar obtained from bone biochar**

### *3.1.3 X-Ray Diffraction (XRD)*

The XRD pattern of bone biochar (Fig. 3) reveals a dual-phase structure comprising disordered aromatic carbon (broad 002 peak) and crystalline hydroxyapatite (101, 200, 220, 300, 311 peaks). The coexistence of crystalline and amorphous phases indicates partial graphitization alongside mineral stabilization during pyrolysis.

The carbon phase may facilitate PAH adsorption through π–π interactions, hydrophobic partitioning, and pore filling (Ahmad *et al*., 2014; Wang & Wang, 2019), while the hydroxyapatite phase immobilizes $Cd^{2+}$, $Ni^{2+}$, $Pb^{2+}$ via ion exchange, surface complexation, and precipitation (Tan *et al*., 2015; Li *et al*., 2017). Chromium (VI) is reduced to Cr (III) and subsequently bound to the biochar surface (Wang & Wang, 2019).

This redox-assisted immobilization further enhances long-term contaminant stability in soil environments. This dual functionality makes bone biochar particularly effective for remediating crude-oil contaminated soils containing both organic pollutants and heavy metals.

The dual-phase composition explains the simultaneous removal efficiency observed for both hydrophobic organic pollutants and metal ions.

### *3.2 Dose-Dependent Sorption Effects of Biochar on PAHs and Selected Heavy Metals of Crude Oil Contaminated Soil*

Adsorption experiments were designed to evaluate how increasing adsorbent dosage influences contaminant removal efficiency and adsorption equilibrium behavior.

#### *3.2.1 Bone Biochar (Bb) Dosage on PAHs Sorption on Crude Oil Contaminated Soil*

Table 1 demonstrates dose-dependent PAH reduction by bone biochar (BB), with total PAHs decreasing from 47.11 mg/kg (control) to 4.90 mg/kg at 10 g BB (89.6% removal). This progressive reduction reflects increased site availability with dosage (Ahmad *et al*., 2014; Mohan *et al*., 2014; Tan *et al*., 2015). Increasing dosage enhances the probability of adsorbate–adsorbent interactions by providing additional active binding sites and reducing competition among PAH molecules.

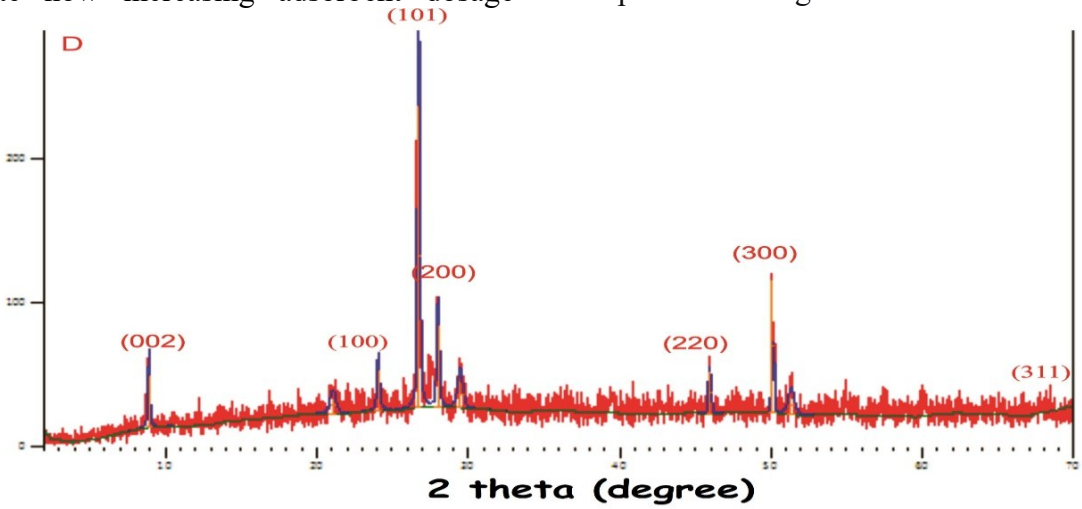


**Fig. 3: The X-ray diffraction pattern of biochar obtained from bone biochar**

Removal efficiencies across 16 priority PAHs ranged narrowly (89.11–89.75%), indicating uniform adsorption of both LMW and HMW congeners via BB's aromatic domains, microporous structure, and π–π interactions (Leng *et al*., 2021; Wang *et al*., 2020; Zhang *et al*., 2017). LMW PAHs adsorbed through pore-filling, while HMW PAHs partitioned hydrophobically onto condensed aromatic structures (Wang *et al*., 2020). BB's mineral phases (hydroxyapatite) may enhance sorption via surface complexation (Ahmad *et al*., 2014; Wang *et al*., 2020). The consistent removal across molecular weights indicates that pore accessibility and aromatic surface chemistry were sufficiently optimized in the produced biochar. Low standard deviations confirm reproducible immobilization (Tan *et al*., 2015). The 89–90% removal across all EPA priority PAHs establishes BB as an effective, sustainable sorbent for petroleum-contaminated soil remediation (Leng *et al*., 2021; Wang *et al*., 2020).

#### *3.2.2 Bone Biochar (BB) Dosage on Some Selected Heavy Metals Sorption on Crude Oil Contaminated Soil*

Heavy metal immobilization behavior was evaluated to determine the effectiveness of mineral-rich biochar phases under hydrocarbon-impacted soil conditions. The results presented in Table 2 demonstrate a clear dose dependent reduction in heavy metal concentrations following the application of bone biochar (BB) to crude oil contaminated soil. These findings demonstrate that bone biochar maintains adsorption selectivity while achieving high removal efficiency across structurally diverse PAH compounds.

**Table 1: Effects of Bone Biochar (Bb) Dosage on PAHs Sorption on Crude Oil Contaminated Soil.**

| S/N | 16 Priority PAH Congeners | CONTROL SOIL | BB (2g) | BB (4g) | BB (6g) | BB (8g) | BB (10g) | % adsorbed 10g |
|---|---|---|---|---|---|---|---|---|
| 1 | **Naphthalene** | 5.01 ±0.01 | 3.10 ±0.11 | 1.57 ±0.02 | 1.08 ±0.02 | 0.62 ±0.01 | 0.52 ±0.01 | 89.62 |
| 2 | **Acenaphthylene** | 2.56 ±0.00 | 1.58 ±0.22 | 0.80 ±0.04 | 0.55 ±0.04 | 0.32 ±0.03 | 0.27 ±0.03 | 89.45 |
| 3 | **Acenaphthene** | 5.86 ±0,01 | 3.63 ±0.37 | 1.84 ±0.07 | 1.27±0.06 | 0.72±0.04 | 0.61±0.04 | 89.59 |
| 4 | **Fluorene** | 3.14 ±0.01 | 1.94 ±0.11 | 0.99±0.02 | 0.68 ±0.02 | 0.39 ±0.01 | 0.33 ±0.02 | 89.49 |
| 5 | **Phenanthrene** | 2.03 ±0.01 | 1.26 ±0.07 | 0.64 ±0.01 | 0.50 ±0.01 | 0.25 ±0.01 | 0.21 ±0.02 | 89.66 |
| 6 | **Anthracene** | 2.44 ±0.01 | 1.51 ±0.07 | 0.77 ±0.01 | 0.65 ±0.02 | 0.45 ±0.02 | 0.25 ±0.03 | 89.75 |
| 7 | **Fluoranthene** | 1.01 ±0.01 | 0.63 ±0.07 | 0.32 ±0.02 | 0.22 ±0.01 | 0.19 0.01 | 0.11 ±0.01 | 89.11 |
| 8 | **Pyrene** | 1.44 ±0.01 | 0.89 0.11 | 0.45 0.02 | 0.31 ±0.01 | 0.18 ±0.01 | 0.15 ±0.01 | 89.58 |
| 9 | **Benz[a]anthracene** | 2.56 ±0.01 | 1.58 ±0.05 | 0.80 ±0.01 | 0.55 0.01 | 0.32 ±0.01 | 0.27 0.01 | 89.45 |
| 10 | **Chrysene** | 3.82 ±0.01 | 2.36 ±0.06 | 1.20 0.01 | 0.83 ±0.01 | 0.47 ±0.01 | 0.40 ±0.01 | 89.53 |
| 11 | **Benzo[b]fluoranthene** | 4.27 ±0.01 | 2.64 ±0.06 | 1.34 ±0.01 | 0.92±0.01 | 0.53 ±0.01 | 0.45 ±0.01 | 89.46 |
| 12 | **Benzo[k]fluoranthene** | 2.79 ±0.01 | 1.73 ±0.07 | 0.88 ±0.01 | 0.60 ±0.01 | 0.34 ±0.01 | 0.29 ±0.01 | 89.61 |
| 13 | **Benzo[a]pyrene** | 2.19 ±0.01 | 1.36 ±0.05 | 0.69 ±0.01 | 0.47±0.01 | 0.27 ±0.01 | 0.23 ±0.01 | 89.50 |
| 14 | **Indeno[1,2,3-cd]pyrene** | 2.44 ±0.01 | 1.51±0.03 | 0.77 ±0.01 | 0.53±0.01 | 0.30 ±0.01 | 0.25 ±0.01 | 89.75 |
| 15 | **Dibenz[a,h]-anthracene** | 2.55 ±0.01 | 1.58 ±0.03 | 0.80 ±0.01 | 0.55 ±0.01 | 0.31 ±0.01 | 0.27 ±0.01 | 89.41 |
| 16 | **Benzo[ghi]-perylene** | 3.00 ±0.01 | 1.86 ±0.04 | 0.94 ±0.01 | 0.65 ±0.01 | 0.37 ±0.01 | 0.31 ±0.01 | 89.67 |
| | **Total PAH (mg/kg)** | **47.11 ±0.15** | **29.15 ±1.50** | **14.78 ±0.26** | **10.36 ±0.21** | **6.03 ±0.15** | **4.90 ±0.21** | |

**Table 2: Effects of Bone Biochar (Bb) Dosage on Some Selected Heavy Metals Sorption On Crude Oil Contaminated Soil**

| Heavy Metals (mg/kg) | Control Soil | BB (2g) | BB (4g) | BB (6g) | BB (8g) | BB (10g) | % adsorbed @ 10g |
|---|---|---|---|---|---|---|---|
| **Cadmium (Cd)** | 72.56 ±0.01 | 61.40 ±0.09 | 50.32 ±0.75 | 41.94 ±0.08 | 35.23 ±0.58 | 29.92 ±0.60 | 58.77 |
| **Chromium (Cr)** | 63.17 ±0.01 | 45.66 ±0.29 | 38.95 ±0.75 | 30.40 ±0.53 | 23.60 ±0.8 | 17.04 ±0.51 | 73.03 |
| **Nickel (Ni)** | 14.20 ±0.01 | 7.80 ±0.30 | 4.29 ±0.01 | 3.73 ±0.35 | 1.93 ±0.11 | 1.49 ±0.06 | 89.51 |
| **Lead (Pb)** | 207.42 ±0.02 | 165.0 ±0.75 | 121.0 ±0.23 | 89.5 0.05 | 66.7 ±0.30 | 51.19 ±0.3 | 75.32 |

Bone biochar dosage increase from 2–10 g progressively reduced Cd, Cr, Ni, and Pb, with adsorption at 10 g reaching 58.77% (Cd), 73.03% (Cr), 89.51% (Ni), and 75.32% (Pb). Higher loading provides greater surface area and reactive sites for metal immobilization (Basanta & Balasubramanian, 2023; Staroń *et al*., 2024). Variations in removal efficiency reflect differences in ionic radius, hydration energy, and affinity for phosphate functional groups. Removal efficiency varied by metal affinity for hydroxyapatite: Pb and Cr formed stable phosphate complexes; Ni (89.51%) adsorbed via ion exchange and electrostatic interactions; Cd (58.77%) showed lower removal due to higher mobility and weaker binding in hydrocarbon-impacted soils (Brazdis *et al*., 2021; Hart *et al*., 2023; Basanta & Balasubramanian, 2023; Viotti *et al*., 2024). Results confirm BB as an effective immobilizing agent for heavy metals in oil-contaminated soils, supporting sustainable remediation (Hart *et al*., 2023; Staroń *et al*., 2024; Viotti *et al*., 2024). The results indicate that adsorption mechanisms are metal-specific but collectively enhanced by hydroxyapatite-driven chemical stabilization.

### *3.3 Adsorption Isotherm Analysis for PAHs and Some Selected Heavy Metals*

Adsorption isotherm modeling was employed to quantify adsorption capacity and to identify dominant interaction mechanisms between contaminants and bone biochar surfaces.

Baseline contaminant concentrations ($C_0$) were established from the untreated control soil tables 1 and 2: Pahs (47.11 mg/kg), cadmium. These parameters enabled comparison of theoretical adsorption assumptions with experimental observations.

m (72.56 mg/kg), chromium (63.17 mg/kg), nickel (14.20 mg/kg), and lead (207.42 mg/kg). Equilibrium concentrations ($C_e$) were recorded following bone biochar treatment at various dosages, and adsorption capacity ($q_e$) was computed for each isotherm model.

Collectively, the isotherm results confirm that physical adsorption supported by microporous structure dominates PAH immobilization.

#### *3.3.1 Adsorption Isotherm Analysis for PAHs Using Bone Biochar (BB)*

The 16-priority poly cyclic aromatic hydrocarbons (PaAHs) adsorption onto bone biochar (BB) as observed from the isotherm data in table 3, 4, and 5 followed the Langmuir model ($R^2$ = 0.988) most closely, indicating monolayer coverage on homogeneous,

energetically equivalent sites via micropore filling and π–π interactions with graphitic domains (Chen *et al*., 2022; Li *et al*., 2014). The Temkin ($R^2$ = 0.956) and Freundlich ($R^2$ = 0.938) models showed good but lower correlations, suggesting secondary roles for surface heterogeneity and decreasing adsorption energy with coverage. This model hierarchy (Langmuir > Temkin > Freundlich) confirms monolayer adsorption and pore-filling as dominant mechanisms, with minor contributions from adsorbate–adsorbate interactions, consistent with recent literature (Jelena *et al*., 2025).

**Table 3: Langmuir Isotherm Data For Pahs Using Bone Biochar (Ypb)**

| Ce (mg/kg) | qe (mg/kg·g$^{-1}$) | Ce/qe |
|---|---|---|
| 29.15 | 8.9800 | 3.2461 |
| 14.78 | 8.0825 | 1.8286 |
| 10.36 | 6.1250 | 1.6914 |
| 6.03 | 5.1350 | 1.1743 |
| 4.90 | 4.2210 | 1.1609 |

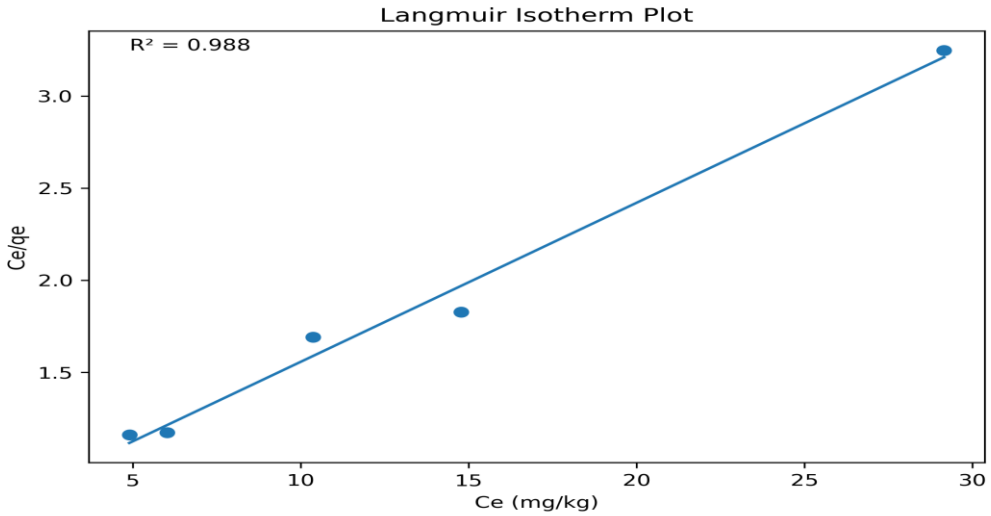


**Fig. 4: Langmuir isotherm for PAHs adsorption using bone biochar (BB)**

**Table 4: Freundlich Isotherm Data For PAHs # (BB)**

| Ce (mg/kg) | qe (mg/kg·g$^{-1}$) | log Ce | log qe |
|---|---|---|---|
| 29.15 | 8.9800 | 1.4646 | 0.9533 |
| 14.78 | 8.0825 | 1.1697 | 0.9075 |
| 10.36 | 6.1250 | 1.0154 | 0.7871 |
| 6.03 | 5.1350 | 0.7803 | 0.7105 |
| 4.90 | 4.2210 | 0.6902 | 0.6254 |

### *3.3.2 Adsorption Isotherm Analysis for Some Selected Heavy Metals Using Bone Biochar (BBs)*

Isotherm data for Langmuir, Freundlich, and Temkin models for cadmium adsorption onto bone biochar (BB) in table 6 and Fig. 7 was best described by the Langmuir model ($R^2$ = 0.9779; $q_{max} \approx 8.08$ mg·kg$^{-1}$), indicating monolayer coverage on homogeneous active sites via chemisorption interactions between $Cd^{2+}$ and BB's functional groups or mineral phases (Romanus *et al*., 2025; Farzi *et al*., 2018). Freundlich ($R^2$ = 0.9277) and Temkin ($R^2$ = 0.9356) fits revealed additional contributions from surface heterogeneity, variable binding energies, and decreasing

adsorption heat with coverage. These models collectively demonstrate that Cd uptake involves multiple mechanisms, which include monolayer adsorption, complexation, ion exchange, and surface precipitation, which are consistent with biochar heavy metal sorption studies (Senthilkumar & Mogili Reddy Prasad, 2020; Wei *et al*., 2025).

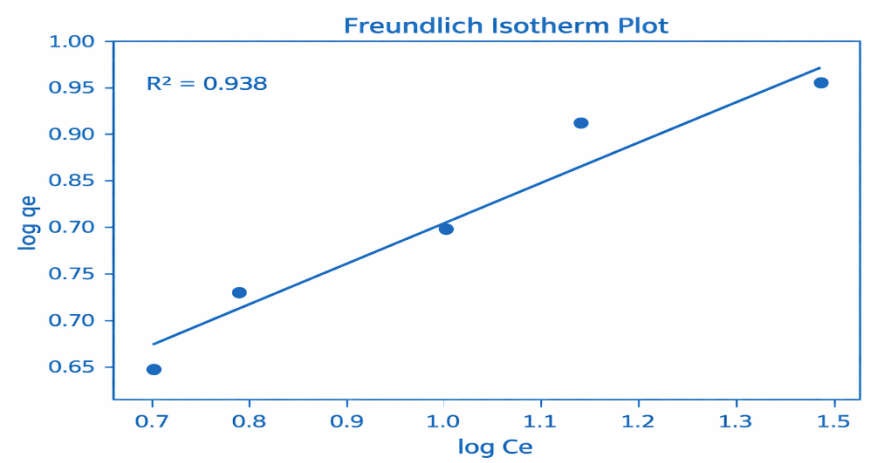


**Fig. 5: Freundlich isotherm for PAHs adsorption using bone biochar (BB)**

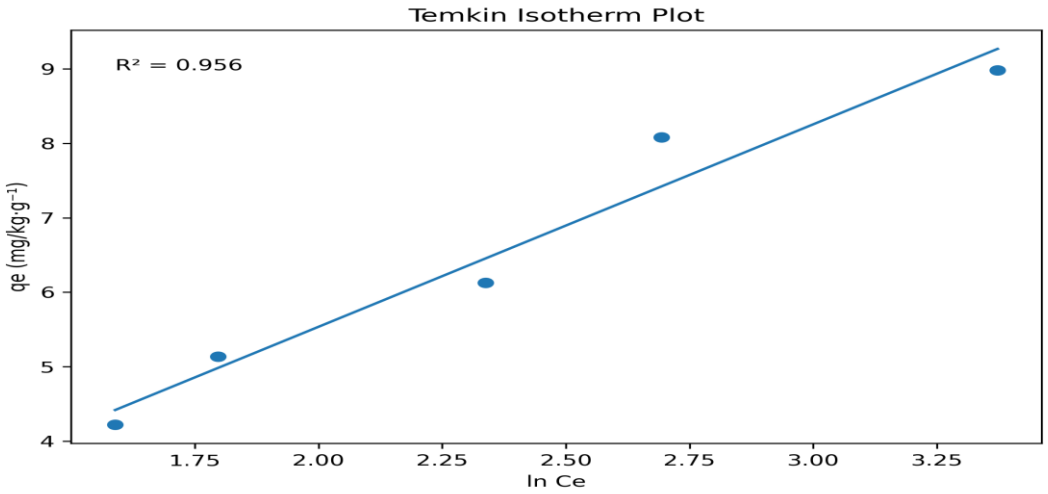


**Fig. 6: Temkin isotherm for PAHs adsorption using bone biochar (BB)**

**Table 5: Temkin Isotherm Data for Pahs Using Bone Biochar (BB).**

| Ce (mg/kg) | ln Ce | qe (mg/kg·g⁻¹) |
|---|---|---|
| 29.15 | 3.3725 | 8.9800 |
| 14.78 | 2.6933 | 8.0825 |
| 10.36 | 2.3380 | 6.1250 |
| 6.03 | 1.7967 | 5.1350 |
| 4.90 | 1.5892 | 4.2210 |

Chromium observed in the isotherm data in Table7, adsorption onto bone biochar (BB) in crude oil contaminated soil was poorly described by the Langmuir model ($R^2$ =

0.5373), despite an appreciable maximum capacity ($q_{max}$ ≈ 15.51 mg/g), indicating that adsorption does not follow monolayer coverage on homogeneous surfaces. The Freundlich model provided a better fit ($R^2$ = 0.7875), confirming heterogeneous surface interactions with varying binding energies, consistent with bone biochar's complex mineral and functional group composition (Ahmad *et al*., 2022; Wei *et al*., 2025s).

**Table 6: Langmuir, Freundlich and Temkin Isotherm Data for Cadmium Using Bone Biochar (BB)**

| Dosage (g) | Ce (mg/kg) | qe (mg/g) | Langmuir Ce/qe | Freundlich logCe | Freundlich logqe | Temkin lnCe |
|---|---|---|---|---|---|---|
| 2.0 | 61.4 | 5.58 | 11.0036 | 1.7882 | 0.7466 | 4.1174 |
| 4.0 | 50.32 | 5.56 | 9.0504 | 1.7017 | 0.7451 | 3.9184 |
| 6.0 | 41.94 | 5.1033 | 8.2182 | 1.6226 | 0.7079 | 3.7362 |
| 8.0 | 35.23 | 4.6663 | 7.55 | 1.5469 | 0.669 | 3.5619 |
| 10.0 | 29.92 | 4.264 | 7.0169 | 1.476 | 0.6298 | 3.3985 |

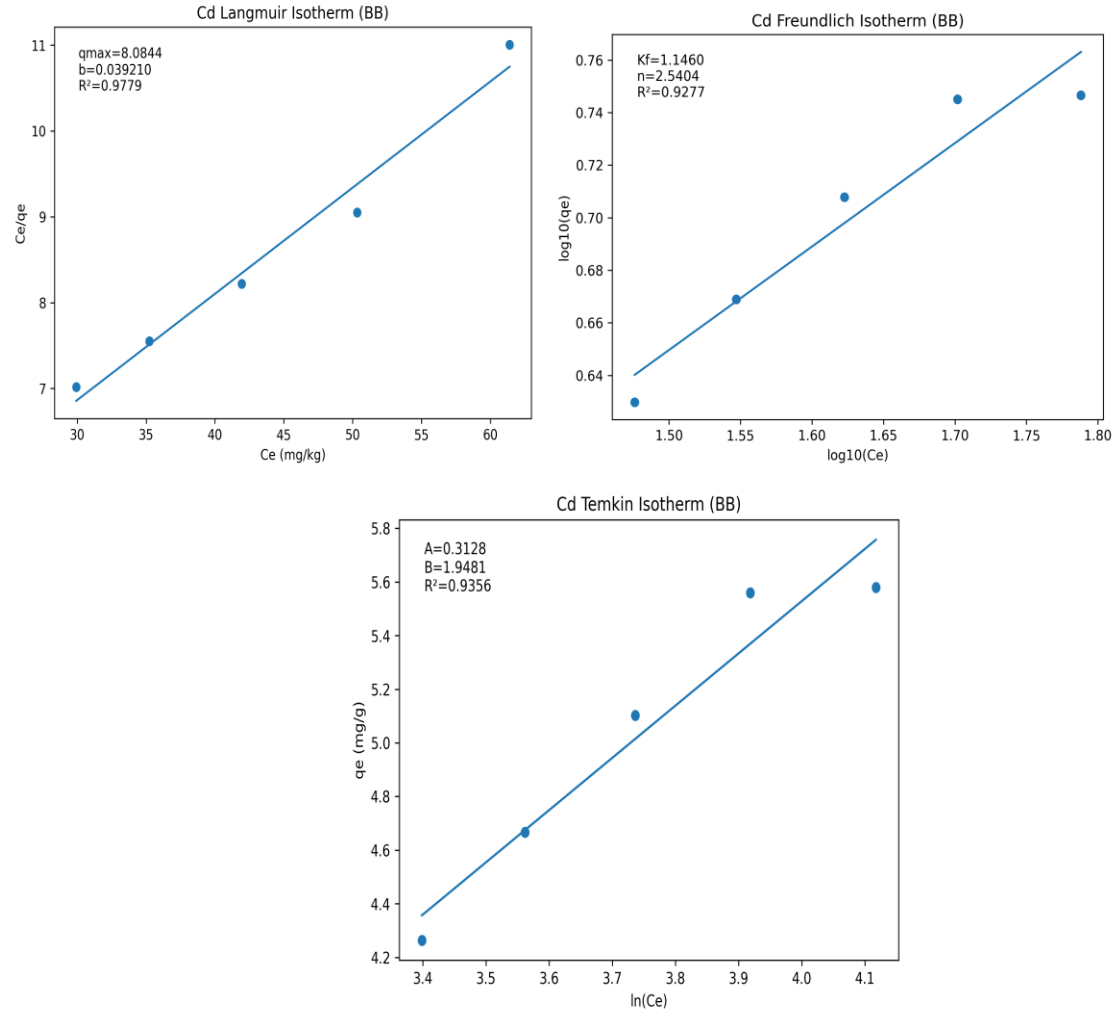


**Fig. 7: Langmuir, Freundlich and Temkin isotherms for cadmium adsorption using bone biochar (BB)**

**Table 7: Langmuir, Freundlich and Temkin Isotherm Data for Chromium Using Bone Biochar (Bb)**

| Dosage (g) | Ce (mg/kg) | qe (mg/g) | Langmuir Ce/qe | Freundlich logCe | Freundlich logqe | Temkin lnCe |
|---|---|---|---|---|---|---|
| 2.0 | 45.66 | 8.755 | 5.2153 | 1.6595 | 0.9423 | 3.8212 |
| 4.0 | 38.95 | 6.055 | 6.4327 | 1.5905 | 0.7821 | 3.6623 |
| 6.0 | 30.4 | 5.4617 | 5.5661 | 1.4829 | 0.7373 | 3.4144 |
| 8.0 | 23.6 | 4.9462 | 4.7713 | 1.3729 | 0.6943 | 3.1612 |
| 10.0 | 17.04 | 4.613 | 3.6939 | 1.2315 | 0.664 | 2.8356 |

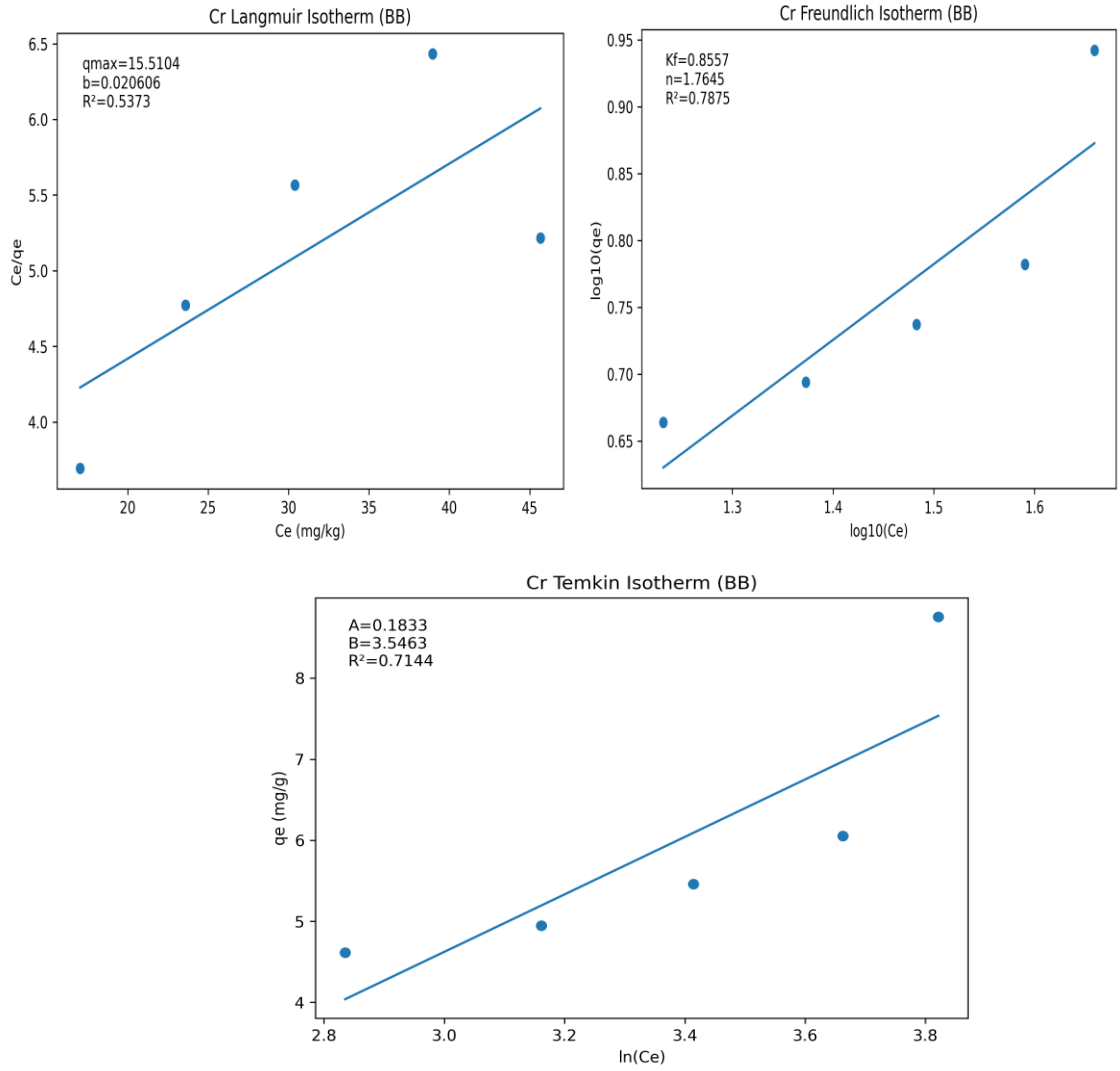


**Fig. 8: Langmuir, Freundlich and Temkin isotherm for chromium adsorption using bone biochar**

The Temkin isotherm ($R^2 = 0.7144$) supported adsorbate–adsorbent interactions, suggesting that electrostatic forces, ion exchange, and surface complexation contribute to Cr immobilization. Hydrocarbons in contaminated soils may modify surface

accessibility and Cr speciation, promoting variable adsorption energies. Bone biochar's calcium phosphate content enhances Cr stabilization through precipitation and complexation (Li *et al*., 2014; Wangwang *et al*., 2024). Overall, Cr adsorption onto BB is governed by heterogeneous surface interactions and chemisorption, supporting its effectiveness in hydrocarbon-impacted soils

**Table 8: Langmuir, Freundlich and Temkin Isotherm Data for Nickel Using Bone Biochar (Bb)**

| Dosage (g) | Ce (mg/kg) | qe (mg/g) | Langmuir Ce/qe | Freundlich logCe | Freundlich logqe | Temkin lnCe |
|---|---|---|---|---|---|---|
| 2.0 | 7.8 | 3.2 | 2.4375 | 0.8921 | 0.5051 | 2.0541 |
| 4.0 | 4.29 | 2.4775 | 1.7316 | 0.6325 | 0.394 | 1.4563 |
| 6.0 | 3.73 | 1.745 | 2.1375 | 0.5717 | 0.2418 | 1.3164 |
| 8.0 | 1.93 | 1.5338 | 1.2584 | 0.2856 | 0.1858 | 0.6575 |
| 10.0 | 1.49 | 1.271 | 1.1723 | 0.1732 | 0.1041 | 0.3988 |

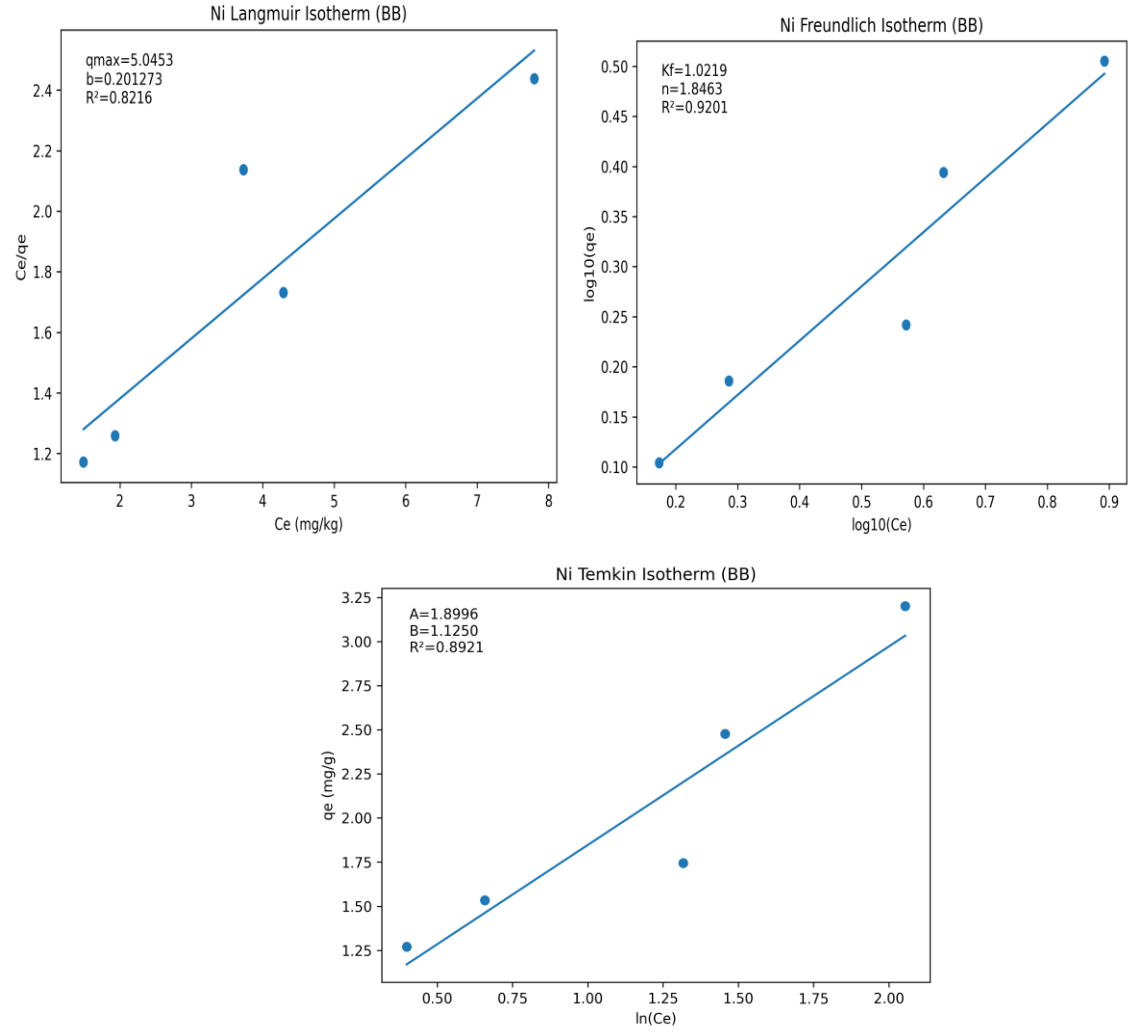


**Fig. 9: Langmuir, Freundlich and Temkin isotherms for nickel adsorption using bone biochar (BB).**

**Table 9: Langmuir, Freundlich and Temkin Isotherm Data For Lead Using Bone Biochar (Bb)**

| Dosage (g) | Ce (mg/kg) | qe (mg/g) | Langmuir Ce/qe | Freundlich logCe | Freundlich logqe | Temkin lnCe |
|---|---|---|---|---|---|---|
| 2.0 | 165.0 | 21.21 | 7.7793 | 2.2175 | 1.3265 | 5.1059 |
| 4.0 | 121.0 | 21.605 | 5.6006 | 2.0828 | 1.3346 | 4.7958 |
| 6.0 | 89.5 | 19.6533 | 4.5539 | 1.9518 | 1.2934 | 4.4942 |
| 8.0 | 66.7 | 17.59 | 3.7919 | 1.8241 | 1.2453 | 4.2002 |
| 10.0 | 51.19 | 15.623 | 3.2766 | 1.7092 | 1.1938 | 3.9355 |

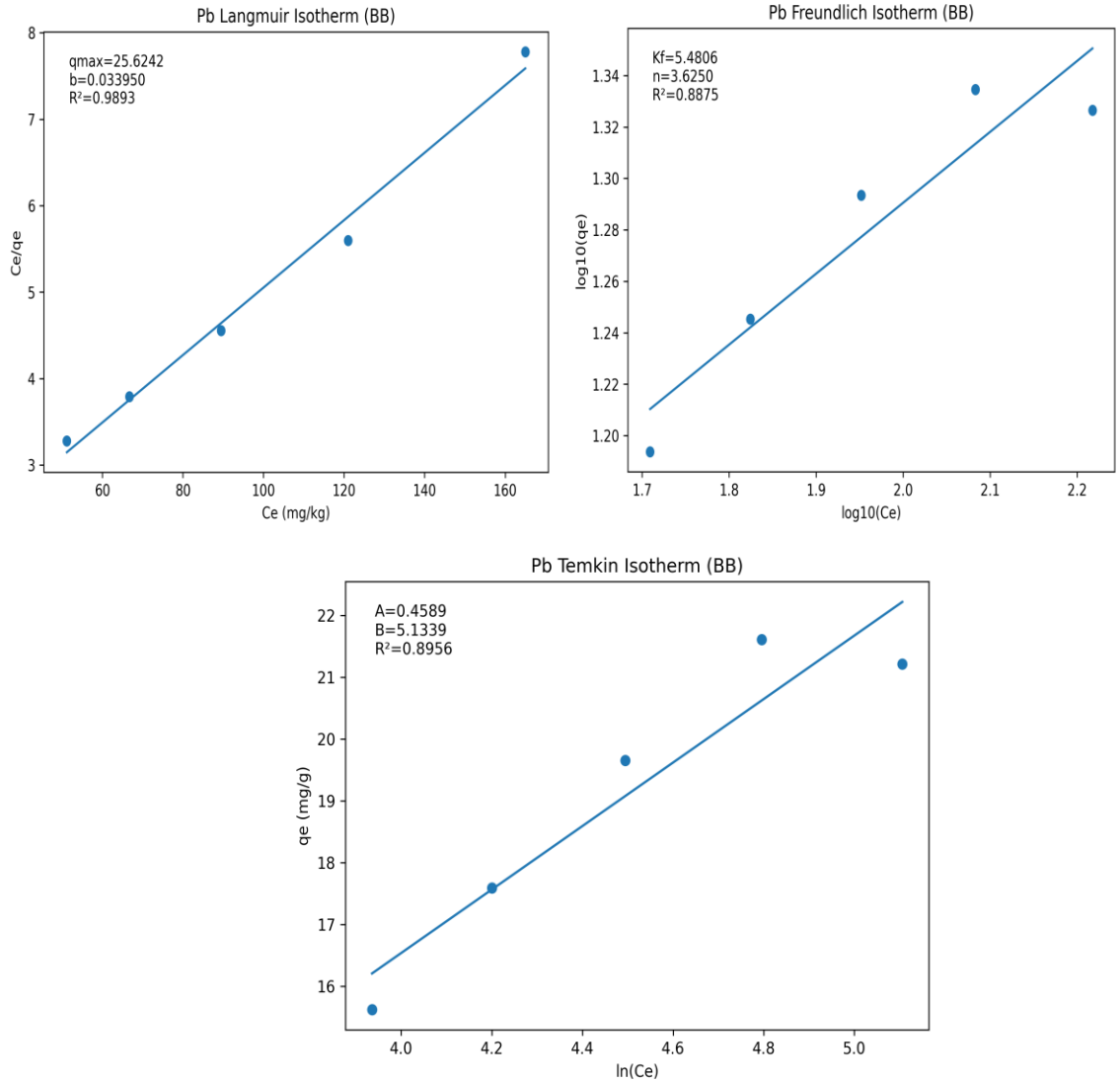


**Fig. 10: Langmuir, Freundlich and Temkin isotherms for lead adsorption using bone biochar (BB).**

The three models for lead adsorption onto bone biochar (BB) in table 9 and Fig. 10 showed that adsorption onto bone biochar (BB) best fit Langmuir model ($R^2$ = 0.9893; $q_{max} \approx 25.62$ mg/kg), confirming monolayer chemisorption on homogeneous sites via surface

complexation and precipitation with hydroxyapatite and carbonate phases (He *et al*., 2022; Mohan *et al*., 2018). Freundlich ($R^2$ = 0.8875) and Temkin ($R^2$ = 0.8956) fits were secondary, with Temkin indicating decreasing adsorption heat with coverage. BB's calcium phosphates enhance Pb stabilization through ion exchange and insoluble lead phosphate formation (Wang *et al*., 2020; Wang *et al*., 2026). Strong chemisorption and mineral-driven precipitation make BB effective for Pb removal in hydrocarbon-impacted soils.

## 4.0 Conclusion

This study systematically evaluated the suitability of bone-derived biochar as a remediation material for soils co-contaminated with polycyclic aromatic hydrocarbons (PAHs) and heavy metals, a widespread environmental concern in oil-producing regions. The biochar synthesized through the pyrolysis of cattle bones at 400 °C exhibited a distinctive dual-phase architecture composed of a porous carbon framework integrated with crystalline hydroxyapatite, as confirmed by SEM, FTIR, and XRD analyses. This hybrid structure provided complementary adsorption functionalities, enabling simultaneous sequestration of organic pollutants through carbon-mediated interactions and immobilization of metal ions via mineral-associated binding mechanisms. Experimental assessment involving biochar dosages ranging from 2 g to 10 g demonstrated a clear dose-dependent enhancement in contaminant removal efficiency, with maximum remediation performance achieved at the highest application rate. The removal of sixteen priority PAHs and four heavy metals (Cd, Cr, Ni, and Pb) confirmed the broad-spectrum adsorption capability of the material.

Mechanistic interpretation using Langmuir, Freundlich, and Temkin isotherm models revealed distinct adsorption pathways depending on contaminant type. The adsorption of PAHs, cadmium, and lead was best described by Langmuir-type behavior, indicating predominately monolayer chemisorption on energetically uniform sites of the biochar surface. In contrast, chromium and nickel adsorption followed heterogeneous surface interactions consistent with Freundlich-type behavior, suggesting the involvement of multiple binding sites and mechanisms, including surface complexation and mineral-assisted adsorption. These findings highlight that adsorption performance is governed not only by biochar dosage but also by pollutant-specific physicochemical interactions, emphasizing the importance of mechanistic understanding in optimizing remediation strategies.

Overall, the study concludes that bone-derived biochar is an effective, sustainable, and multifunctional adsorbent for the simultaneous remediation of mixed organic and inorganic contaminants in polluted soils. The synergistic combination of porous carbon and hydroxyapatite phases provides enhanced adsorption versatility, making the material particularly suitable for complex contamination scenarios typical of petroleum-impacted environments. The results further demonstrate that appropriate dosage optimization and recognition of contaminant-specific adsorption mechanisms are critical parameters for achieving efficient large-scale soil remediation.

However, the conclusions drawn from this work are based on controlled laboratory batch experiments, which may not fully replicate the dynamic physicochemical and biological conditions encountered in field environments. It is therefore recommended that future investigations focus on long-term column studies and pilot-scale field trials to evaluate adsorption stability, ageing effects, and performance under variable environmental conditions, including moisture fluctuations, microbial activity, and competing ions. Additional studies should also examine regeneration potential, desorption behavior, and life-cycle economic assessments to

determine the long-term feasibility and sustainability of bone biochar deployment. Advancing these aspects will support the translation of laboratory findings into practical, scalable remediation technologies for contaminated soils in oil-producing regions.

## 5.0 Acknowledgement

The authors acknowledge the support received from the laboratory staff personnel in the department of chemistry, Federal University of Petroleum Resources, Effurun, and the Staff and manager of Jacio environmental limited for their technical and immense support.

## 5.0 References

Ahmad, M., Rajapaksha, A. U., Lim, J. E., Zhang, M., Bolan, N., Mohan, D., Vithanage, M., Lee, S. S., & Ok, Y. S. (2014). Biochar as a sorbent for contaminant management in soil and water: A review. *Chemosphere*, 99, pp. 19–33. https://doi.org/10.1016/j.chemosphere.2013.10.071

Akpanudo, N. W., & Chibuzo, O. U. (2020). *Musanga cecropioides* sawdust as an adsorbent for the removal of methylene blue from aqueous solution. *Communication in Physical Sciences*, 5, 3, pp. 362–370.

Akpanudo, N. W., & Olabemiwo, O. M. (2024a). Green synthesis and characterization of copper nanoparticles (CuNPs) and composites (CuC) using the *Echinochloa pyramidalis* extract and their application in the … *Water Practice & Technology*, 19, 2*, pp.* 324–342.

Akpanudo, N. W., & Olabemiwo, O. M. (2024b). Synthesis and characterization of silver nanoparticles and nanocomposites using *Echinochloa pyramidalis* (Antelope grass) plant parts and the application of the nanocomposite … *South African Journal of Chemical Engineering*, 47, 1, pp. 98–110.

Akpanudo, N. W., Akpakpan, A. E., Nsi, E. W., Akpan, N. A., & Umana, I. A. (2024). Application of activated carbon prepared from nypa palm seed husk in the adsorption of azo dyes from waste water and evaluation of the adsorption isotherms. *Journal of Materials Science Research and Reviews*, 7, 2*, pp.* 210–217.

Awaka-Ama, J. J., Udo, G. J., Uwanta, E. J., Etukudo, N. J., Akpanudo, N. W., & Igwe, R. (2024). Comparative analysis of heavy metal contamination in regular and artisanal petroleum products in Akwa Ibom State, South-South Nigeria. *Communication in Physical Sciences*, 11, 3, pp. 559–568.

Basanta, K. B., & Balasubramanian, R. (2023). Use of biochar as a low-cost adsorbent for removal of heavy metals from water and wastewater: A review. *Journal of Environmental Chemical Engineering*, 11, 5, pp. 110986–110986. https://doi.org/10.1016/j.jece.2023.110986

Bayar, J., Ali, N., Dong, Y., Ahmad, U., Anjum, M. M., Khan, G. R., Zaib, M., Jalal, A., Ali, R., & Ali, L. (2024). Biochar-based adsorption for heavy metal removal in water: A sustainable and cost-effective approach. *Environmental Geochemistry and Health*, 46, 11. https://doi.org/10.1007/s10653-024-02214-w

Brazdis, R. I., Fierascu, I., Avramescu, S. M., & Fierascu, R. C. (2021). Recent progress in the application of hydroxyapatite for heavy metals from water matrices. *Materials*, 14, 22, pp. 6898–6898. https://doi.org/10.339/ma14226898

Chen, Q., Zhang, Z., Wang, Y., Mu, G., Wu, X., Liu, Y., Luo, W., & Wen, X. (2022). Remediation of soil contaminated by heavy metals using biochar: Strategies and future prospects. *Polish Journal of Environmental Studies*, 32, 1, pp. 27–40. https://doi.org/10.15244/pjoes/153912

Das, S. K. (2024). Adsorption and desorption capacity of different metals influenced by biomass derived biochar. *Environmental Systems Research*, 13, 1. https://doi.org/10.1186/s40068-024-00335-w

Eddy, N. O., Garg, R., Garg, R., Ukpe, R. A. & Abugu, H. (2023b). Adsorption and photodegradation of organic contaminants by silver nanoparticles: isotherms, kinetics, and computational analysis. *Environmental Monitoring and Assessment*,, DOI : 10.1007/s10661-023-12194-6,

Eddy, N. O., Garg, R., Garg, R., Ukpe, R. A. & Abugu, H. (2023c). Adsorption and photodegradation of organic contaminants by silver nanoparticles: isotherms, kinetics, and computational analysis. *Environmental Monitoring and Assessment*,, DOI : 10.1007/s10661-023-12194-6,

Eddy, N. O., Garg, R., Ukpe, R. A., Akpanudo, N. W., Abugu, H., Garg, R., Anjum, A. & Anand, B. (2024a). Chapter Ethical issues Chapter 10: Ethical and environmental implications associated with the application of nanoparticles. doi:: 10.4018/979-8-3693-1094-6.ch010. pp. 274-299.

Eddy, N. O., Oladede, J., Eze, I. S., Garg, R., Garg, R., & Paktin, H. (2024b). Synthesis and characterization of CaO nanoparticles from periwinkle shell for the treatment of tetracycline-contaminated water by adsorption and photocatalyzed degradation. *Results in Engineering*, *103374*. https://doi.org/10.1016/j.rineng.2024.103374.

Eddy, N. O., Ukpe, R. A., Garg, R., Garg, R., Odionenyi A. O., Ameh, P. & Akpet, I, N. (2023a). Enhancing Water Purification Efficiency through Adsorption and Photocatalysis: Models, Application and Challenges. *International Journal of Environmental Analytical Chemistry*, DOI: 10.1080/03067319.2023.2295934

Farzi, S., Farasati, M., Bansouleh, B. F., & Pirsaheb, M. (2018). Evaluation of batch and continuous adsorption kinetic models of cadmium from aqueous solutions using sugarcane straw nano-structure absorbent. *Desalination and Water Treatment*, 115, pp. 135–144. https://doi.org/10.5004/dwt.2018.22450

Haris, M., Amjad, Z., Usman, M., Saleem, A., Ainur, D., Mahmood, Z., Dina, K., Guo, J., & Wang, W. (2024). A review of crop residue-based biochar as an efficient adsorbent to remove trace elements from aquatic systems. *Biochar*, 6, 1. https://doi.org/10.1007/s42773-024-00341-2

Hart, A., Porbeni, D. W., Omonmhenle, S., & Peretomode, E. (2023). Waste bone char-derived adsorbents: Characteristics, adsorption mechanism and model approach. *Environmental Technology Reviews*, 12, 1, pp. 175–204. https://doi.org/10.1080/21622515.2023.2197128

Jelena, B., Marijana, K. I., Jasmina, A., Maja, V., Snežana, M., & Aleksandra, T. (2025). Adsorptive behavior of corn-cob- and straw-derived biochar for polycyclic aromatic hydrocarbon removal from aqueous systems. *Processes*, 13, 5, pp. 1521–1521. https://doi.org/10.3390/pr13051521

Kelle, H. I., Ogoko, E. C., Akintola O & Eddy, N. O. (2023). Quantum and experimental studies on the adsorption efficiency of oyster shell–based CaO nanoparticles (CaONPO) towards the removal of methylene blue dye (MBD) from aqueous solution. *Biomass Conversion and Biorefinery,* 14, 31925–31948. https://doi.org/10.1007/s13399-023-04947-7.

Leng, L., Xiong, Q., Yang, L., Li, H., Zhou, Y., Zhang, W., & Jiang, S. (2021). An

overview on engineering the surface area and porosity of biochar. *Science of the Total Environment*, 763, pp. 144204–144204. https://doi.org/10.1016/j.scitotenv.2020.144204

Li, H., Dong, X., da Silva, E. B., de Oliveira, L. M., Chen, Y., & Ma, L. Q. (2017). Mechanisms of metal sorption by biochars: Biochar characteristics and modifications. *Chemosphere*, 178, pp. 466–478. https://doi.org/10.1016/j.chemosphere.2017.03.072

Li, J., Zheng, L., Wang, S.-L., Wu, Z., Wu, W., Niazi, N. K., Shaheen, S. M., Rinklebe, J., Bolan, N., Kim, K.-H., & Wang, H. (2019). Sorption mechanisms of lead on silicon-rich biochar in aqueous solution: Spectroscopic investigation. *Science of the Total Environment*, 672, pp. 572–582. https://doi.org/10.1016/j.scitotenv.2019.04.003

Li, Y., Liu, J., Wei, B., Zhang, X., Liu, X., & Han, L. (2024). A comprehensive review of bone char: Fabrication procedures, physicochemical properties, and environmental application. *Science of the Total Environment*, 954, pp. 176375–176375. https://doi.org/10.1016/j.scitotenv.2024.176375

Li, Y., Shao, J., Wang, X., Deng, Y., Yang, H., & Chen, H. (2014). Characterization of modified biochars derived from bamboo pyrolysis and their utilization for target component (furfural) adsorption. *Energy & Fuels*, 28, 8, pp. 5119–5127. https://doi.org/10.1021/ef500725c

Mei, H., Huang, W., Wang, Y., Xu, T., Zhao, L., Zhang, D., Luo, Y., & Pan, X. (2022). One stone two birds: Bone char as a cost-effective material for stabilizing multiple heavy metals in soil and promoting crop growth. *Science of the Total Environment*, 840, pp. 156163–156163. https://doi.org/10.1016/j.scitotenv.2022.156163

Meng, F., Wang, Y., & Wei, Y. (2025). Advancements in biochar for soil remediation of heavy metals and/or organic pollutants. *Materials*, 18, 7, pp. 1524–1524. https://doi.org/10.3390/ma18071524

Mohan, D., Abhishek, K., Sarswat, A., Patel, M., Singh, P., & Pittman, C. U. (2018). Biochar production and applications in soil fertility and carbon sequestration – A sustainable solution to crop-residue burning in India. *RSC Advances*, 8, 1, pp. 508–520. https://doi.org/10.1039/c7ra10353k

Mohan, D., Sarswat, A., Ok, Y. S., & Pittman, C. U. (2014). Organic and inorganic contaminants removal from water with biochar, a renewable, low-cost and sustainable adsorbent – A critical review. *Bioresource Technology*, 160, pp. 191–202. https://doi.org/10.1016/j.biortech.2014.01.120

Ogoko, E. C., Kelle, H. I., Akintola, O. and Eddy, N. O. (2023). Experimental and theoretical investigation of *Crassostrea* gigas (gigas) shells based CaO nanoparticles as a photocatalyst for the degradation of bromocresol green dye (BCGD) in an aqueous solution. *Biomass Conversion and Biorefinery*. https://doi.org/10.1007/s13399-023-03742-8.

Rodrigues Viana, R. d. S., Chagas, J. K. M., Paz-Ferreiro, J., & Figueiredo, C. C. d. (2025). Enhanced remediation of heavy metal-contaminated soils using biochar and zeolite combinations with additives: A meta-analysis. *Environmental Pollution*, 367, pp. 125617–125617. https://doi.org/10.1016/j.envpol.2024.125617

Romanus, E. N., Chidiebere, M. B., Chioma, C. S., Vincent, U. S., & Ngozi, I. J. (2025). Adsorptive removal of some toxic metal ions from aqueous solution using *Moringa oleifera* root powder biochar: Equilibrium, kinetic and thermodynamic studies. *Environmental Chemistry and Safety*, 1, 2,

pp. 9600007–9600007. https://doi.org/10.26599/ecs.2025.9600007

Senthilkumar, R., & Mogili Reddy Prasad, D. (2020). Sorption of heavy metals onto biochar. *Applications of Biochar for Environmental Safety*. https://doi.org/10.5772/intechopen.92346

Staroń, P., Zawadzka, A., Radomski, P., & Chwastowski, J. (2024). Characteristics of removal of lead, cadmium and chromium from soil using biosorbent and biochar. *Applied Sciences*, 14, 16, pp. 7241–7241. https://doi.org/10.3390/app14167241

Tan, X., Liu, Y., Zeng, G., Wang, X., Hu, X., Gu, Y., & Yang, Z. (2015). Application of biochar for the removal of pollutants from aqueous solutions. *Chemosphere*, 125, pp. 70–85. https://doi.org/10.1016/j.chemosphere.2014.12.058

Viotti, P., Simone, M., Antonucci, A., Décima, M. A., Lovascio, P., Tatti, F., & Boni, M. R. (2024). Biochar as alternative material for heavy metal adsorption from groundwaters: Lab-scale (column) experiment review. *Materials*, 17, 4, pp. 809–809. https://doi.org/10.3390/ma17040809

Wang, F., Gao, Z., Xiong, T., Bi, J., & Zhang, C. (2026). Meta-analysis compares the removal of heavy metals in water and soil by modified biochar from biomass solid waste. *Ecological Frontiers*. https://doi.org/10.1016/j.ecofro.2026.01.004

Wang, J., & Wang, S. (2019). Preparation, modification and environmental application of biochar: A review. *Journal of Cleaner Production*, 227, pp. 1002–1022. https://doi.org/10.1016/j.scitotenv.2021.152499

Wang, L., Ok, Y. S., Tsang, D. C. W., Alessi, D. S., Rinklebe, J., Wang, H., Mašek, O., Hou, R., O'Connor, D., & Hou, D. (2020). New trends in biochar pyrolysis and modification strategies: Feedstock, pyrolysis conditions, sustainability concerns and implications for soil amendment. *Soil Use and Management*, 36, 3, pp. 358–386. https://doi.org/10.1111/sum.12592

Wangwang, W., Chen, G., Tian, Q., Liu, C., & Chen, J. (2024). Biochar remediates cadmium and lead contaminated soil by stimulating beneficial fungus *Aspergillus* spp. *Environmental Pollution*, 359, pp. 124601–124601. https://doi.org/10.1016/j.envpol.2024.124601

Wei, Y., Ma, J., Liu, K., Zhang, S., & Wang, J. (2025). Biochar-based remediation of heavy metal-contaminated soils: Mechanisms, synergies, and sustainable prospects. *Nanomaterials*, 15, 19, pp. 1487–1487. https://doi.org/10.3390/nano15191487

Wu, D., Lu, J., Huang, K., Jiang, L., Gao, X., Li, S., Liu, H., & Wu, B. (2024). Adsorption potential, speciation transformation, and risk assessment of Hg-, Cd-, and Pb-contaminated soils using biochar in combination with potassium dihydrogen phosphate. *Molecules*, 29, 10, pp. 2202–2202. https://doi.org/10.3390/molecules29102202

Yaashikaa, P. R., Karishma, S., Kamalesh, R., Saravanan, A., Vickram, A. S., & Anbarasu, K. (2024). A systematic review on enhancement strategies in biochar-based remediation of polycyclic aromatic hydrocarbons. *Chemosphere*, 355, pp. 141796–141796. https://doi.org/10.1016/j.chemosphere.2024.141796

Yang, X., Wan, Y., Zheng, Y., He, F., Yu, Z., Huang, J., Wang, H., Ok, Y. S., Jiang, Y., & Gao, B. (2019). Surface functional groups of carbon-based adsorbents and their roles in the removal of heavy metals from aqueous solutions: A critical review. *Chemical Engineering Journal*, 366, pp. 608–621. https://doi.org/10.1016/j.cej.2019.02.119

Zhang, F., Gao, Y., Gao, Y., & Han, R. (2025). Structure-performance relationship of

biochar for direct degradation of organic pollutants. *Carbon Research*, 4, 1. https://doi.org/10.1007/s44246-025-00219-3

Zhang, H., Chen, C., Gray, E. M., & Boyd, S. E. (2017). Effect of feedstock and pyrolysis temperature on properties of biochar governing end use efficacy. *Biomass and Bioenergy*, 105, pp. 136–146. https://doi.org/10.1016/j.biombioe.2017.06.024

**Declaration**

**Consent for publication**

Not Applicable

**Availability of data and materials**

The publisher has the right to make the data public

**Conflict of Interest**

The authors declared no conflict of interest

**Ethical Considerations**

Not applicable

**Competing interest**

The authors report no conflict or competing interest

**Funding**

The author declared no source of funding

**Authors' Contribution**

Kenneth A. Ibe and Wisdom Ivwurie led the conceptualization, supervision, and validation of the study. Methodology development involved Kenneth A. Ibe, Wisdom Ivwurie, and Emmanuel O. Okorodudu. Investigation, data curation, and formal analysis were conducted by Emmanuel O. Okorodudu and Bamidele H. Akpeji. Sample collection and preparation included Andrew O. Onofuevure. Emmanuel O. Okorodudu prepared the original draft, while all authors contributed to review and editing.